Influence of the data base and algorithmic parameters on the image quality in holographic diffuse LEED

K. Reuter, H. Wedler, M. Ott, and K. Heinz
Lehrstuhl für Festkörperphysik, University of Erlangen-Nürnberg, Staudtstrasse 7, D-91054 Erlangen, Germany

J. A. Vamvakas, X. Chen, and D. K. Saldin
Department of Physics and Laboratory for Surface Studies, University of Wisconsin-Milwaukee, P.O. Box 413, Milwaukee, Wisconsin 53201

(Received 1 August 1996)

A detailed examination of the influence of different parameters used in diffuse low-energy-electron-diffraction holography is presented. Effects due to the finite and discrete character of the data that are input to the method's reconstruction algorithm are investigated, as well as the influence of additional parameters introduced both for the removal of experimental Bragg-spots and for the recently proposed correction for the anisotropy of the reference wave. As a test case, we applied the reconstruction algorithm to simulated data of the disordered adsorption system O/Ni(001). Guidelines for the width and resolution of the data base to be used, as well as for the proper selection of algorithmic parameters are deduced, which should hold also for other and unknown systems of disordered atomic adsorption. Using a parameter configuration optimized according to our results, a well-resolved and fully three-dimensional image of the local adsorption geometry is reconstructed from the data. [S0163-1829(97)05208-9]

I. INTRODUCTION

In order to overcome the difficulties connected with the ''trial and error'' nature of the conventional quantitative analysis of low-energy-electron-diffraction (LEED) data,[1–3] many efforts have been made to develop a *direct* approach to the desired surface crystallographic information contained therein. Besides the direct inversion of measured data using tensor LEED,[4] the holographic interpretation of diffuse diffraction patterns, which develop in the case of disordered adsorption on a crystalline substrate, seems to be a promising proposal in this respect[5] and has triggered a number of subsequent investigations (for a recent review see Ref. 6). Similar to the cases of other electron-emission experiments using, e.g., photoelectrons,[7] Auger electrons,[8] or Kikuchi electrons,[9] the holographic reconstruction of real space images from diffuse LEED (DLEED) data hence provides approximate, but direct and reliable information on the investigated system.

The information sought in DLEED holography consists of the local atomic environment of adsorbates, which form a disordered lattice gas on a crystal surface. The corresponding state-of-the-art algorithms, when applied to systems of atomic adsorbates, are now capable of reconstructing clear images of the local adsorption geometry using a set of diffraction patterns measured at different electron energies. The prior method of Wei and Tong[10] had already been successful, using experimental data,[11] though the latter had to be taken at different angles of incidence in order to reconstruct fully three-dimensional (3D) atomic images. In contrast, the method of Saldin *et al.*[12,13] provides the full 3D information with data taken for normal incidence only. This is due to the introduction of an additional kernel in the reconstruction algorithm, which now takes the form of an energy-dependent Cartesian transform that, to some extent, compensates for the anisotropy of both the reference and object wave. The method was recently abbreviated by the acronym CORRECT (compensated object and reference-wave reconstruction by an energy-dependent Cartesian transform).[6]

The efficacy of the CORRECT algorithm has been proved recently by the successful holographic reconstruction of local adsorption geometries of the disordered adsorption systems O/Ni(001) and K/Ni(001) from experimental DLEED intensities.[6,12] However, in these two applications to experiment, the algorithm's input was predetermined by already existing data sets, which, for various experimental reasons, consisted of DLEED patterns in a significantly lower energy range than the set considered in the earlier theoretical paper of Saldin and Chen.[13] Consequently, the aim of the present paper is to gain a better understanding of the influence of the size and resolution of a data base that could be expected to be measured in practice, as well as of other parameters used in the reconstruction procedure. We will demonstrate the relevance of the different parameters and deduce guidelines on the size of the data base necessary for a reliable reconstruction of an atomic adsorption system of unknown structure. Our present investigations are based on simulated DLEED data for the disordered adsorption system O/Ni(001). However, the results of these investigations have also been verified with simulated data with potassium as an adatom, giving analogous results, even though potassium has a much stronger scattering factor than oxygen. Since these surfaces possess no special features distinguishing them from any other atomic adsorbate system, the results obtained would be expected also to hold more generally, and therefore we shall concentrate on O/Ni(001) in the rest of this paper.

II. THE RECONSTRUCTION ALGORITHM AND ITS DATA BASE PARAMETERS

At low coverages and/or low temperatures, adsorbates are often found to occupy equivalent local sites on a crystalline

surface with, however, long-range order still missing (disordered lattice gas). Due to the resulting lack of periodicity among the adsorbed species, LEED electrons scattered at least once by an adsorbate are detected at all diffraction angles, leading to a diffuse intensity distribution appearing on the screen. Such a DLEED pattern arising from disordered adsorbates can be assumed to be representative of the intensity distribution due to just one single adsorbate on this surface.[14,15] This perception led to the original holographic interpretation of DLEED as proposed by Saldin and de Andres[5] according to which the adsorbate acts as a microscopic beam splitter. Electrons whose final scattering is by an adsorbate form the *reference* wave, while those scattered subsequently by substrate atoms provide the *object* wave. Thus the atomic structure around the adsorbate should be accessible by a simple Fourier transform. Other propagation paths involving substrate scattering only contribute exclusively to the intensities of Bragg spots due to the substrate structure. Consequently, these spot intensities have to be excluded from the reconstruction process.

However, it became clear rather quickly, that two obstacles prevent such an easy access to the crystallographic information:[16] first, the strong multiple scattering of the low-energy electrons is not at all negligible, as in the usual forms of optical holography. Second, those scattering paths leading first to the surface, followed by one final scattering at the adsorbate before leaving towards the detector, represent a contribution to the *reference* wave, which depends on the object. Fortunately, both of these obstacles can be effectively suppressed when using multiple-energy data.

For this, the original holographic integral transform over the angular range of the data as derived by Barton[17] has to be generalized to a three-dimensional integral extended over both angle and energy. This has to be realized in such a way as to pose a stationary phase condition corresponding to a kinematic object wave, thus suppressing the disturbing contributions mentioned. The final and currently used reconstruction algorithm is accordingly of the following form and can be understood intuitively when considering the phase factor of the object wave function:[13,18]

$$U(\mathbf{r}) = \int\int \left(\int K(k_\perp, \mathbf{k}_\parallel; \mathbf{r}) \chi(k_\perp, \mathbf{k}_\parallel) e^{-i(kr - k_\perp z)} dk_\perp \right) \times e^{i\mathbf{k}_\parallel \cdot \mathbf{r}_\parallel} d^2\mathbf{k}_\parallel . \quad (1)$$

$U(\mathbf{r})$ is the reconstructed amplitude at a point specified by the position vector $\mathbf{r}$ relative to an adsorbate atom on the surface and $\mathbf{k}_\parallel$ and $k_\perp$ are the components of the wave vector $\mathbf{k}$ of a detected electron parallel and perpendicular to the surface, z is the component of $\mathbf{r}$ perpendicular to the surface, and

$$\chi(k_\perp, \mathbf{k}_\parallel) = \frac{H(k_\perp, \mathbf{k}_\parallel) - H_{\mathrm{av}}(\mathbf{k}_\parallel)}{H_{\mathrm{av}}(\mathbf{k}_\parallel)} \quad (2)$$

is a function constructed from the diffuse intensities $H(k_\perp, \mathbf{k}_\parallel)$, with

$$H_{\mathrm{av}}(\mathbf{k}_\parallel) = \frac{\int H(k_\perp, \mathbf{k}_\parallel) dk_\perp}{\int dk_\perp} . \quad (3)$$

The measured intensities enter the reconstruction algorithm via the function χ, which enhances the contrast of their variations in energy without affecting the periodicities involved.[10,13] This normalization is performed to filter out the holographic self-interference terms as well as possible contributions from thermal diffuse scattering, which both lead to only a rather smooth background. Finally, the kernel K serves to compensate for the anisotropy of the reference wave and is dealt with further below.

The general form of the algorithm (1) has some similarity to a three-dimensional Fourier transform over a certain volume in $\mathbf{k}$ space. The data acquisition over angle and energy provides input intensities for a range of both direction and magnitude of the electron wave vector $\mathbf{k}$ and hence determines the size of the usable volume. Further, since all experimental data in reality involve finite steps, the number of angles and energies, at which intensities are measured, relates to the resolution in $\mathbf{k}$ space provided to the discrete integral transform. By thinking in terms of the Fourier-transform analogue,[19] it is easy to identify the relevant data base parameters and their probable effects on the images: while the range in angle and energy will correspond to the achievable resolution parallel to the surface (the ''lateral'' resolution) and that perpendicular to the surface (the ''vertical'' resolution), the spacing of the diffraction pattern data, i.e., the resolution with which they are measured, will influence the lateral and vertical dimensions within which no artifacts due to Fourier transform aliasing are to be expected. Above all, as these four parameters (energy and angular range, and energy and angular resolution) represent a direct measure of the total number of intensities used as input to the algorithm, the minimum amount of data necessary for a reliable image reconstruction can be estimated through them. The following sections will therefore give a thorough examination of the influence of the data base parameters on the reconstructed images, thus facilitating the selection of data when applying DLEED holography to unknown systems of atomic adsorption.

III. DATA SIMULATION AND IMAGE PRESENTATION

In order to perform the tests described above, we use a set of DLEED patterns simulated for a Ni(001) surface covered with a disordered arrangement of O atoms adsorbed in hollow sites. The data, calculated by the DLEED program of Saldin and Pendry,[20] were already used to demonstrate the efficacy of the latest improvements in the reconstruction algorithm, i.e., the CORRECT method mentioned above.[6,13] The DLEED patterns were calculated for normal incidence and electron energies between $E = 136.05$ eV ($=5$ hartrees) and $E = 435.36$ eV ($=16$ hartrees) in 13.6 eV ($=0.5$ hartree) intervals. Each diffraction pattern contains the spatial intensity distribution over the maximum 90° polar opening angle (corresponding to the full 180° hemisphere) with an angular resolution corresponding to 8×8 points per Brillouin zone. As demonstrated earlier, clear and almost perfect image reconstructions could be obtained from these data using the CORRECT algorithm.[13]

However, experimental data are not normally available to the extent of the simulated set described above. By reducing

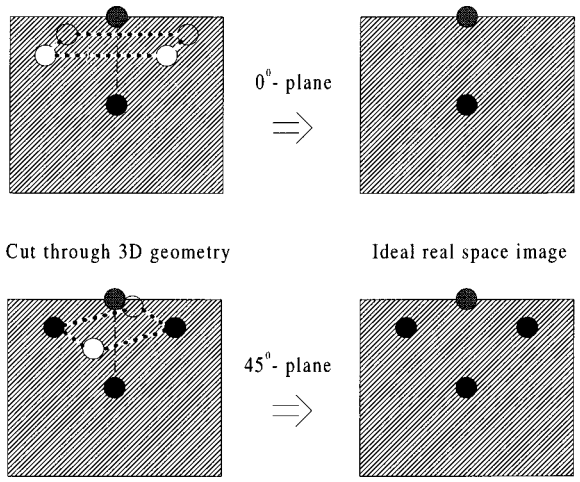

FIG. 1. Schematic model of the O/Ni(001) adsorption geometry and the two high-symmetry cut planes, differing only in a 45° azimuthal angle. Both planes show the fourfold hollow adsorbed O (d_{01}=0.80 Å) at the top and a second layer atom of the bulk-terminated Ni at 2.56 Å below. The 45° plane additionally contains two first layer Ni atoms, when using a reference wave correction. In the following figures, both cut-planes are taken to be 6 Å wide and extend 5 Å in the vertical direction at a resolution of 0.05 Å per pixel.

this data set by variation of the data base parameters, the effect on the image quality—up to the eventual breakdown of the algorithm—can easily be investigated. Proceeding along this line, the optimal parameter configuration obtained, compatible with experimental constraints, can then be used as a general guideline for further applications.

The information desired from holographic DLEED consists in the reconstructed amplitude $U(\mathbf{r})$ over a certain real-space volume around the adsorbate, where high values of $|U(\mathbf{r})|^2$ indicate the position of a substrate atom. For the presentation of results, one is consequently faced with the problem of comprehensively visualizing a three-dimensional scalar field. Two approaches to this can be found in the literature so far: (a) a perspective view of the complete 3D geometry around the adsorbate depicting high image intensity loci with scaled spheres or (b) selected high-symmetry cut planes through the geometry where different intensity values are distinguished by different gray shading. Whereas (a) immediately provides a visual understanding of the adsorbate's environment, (b) can better be used for an exact analysis of the holographic images, however, at the expense of losing the 3D impression. Since we want to compare quantitatively results based on different data sets, visualization (b) is chosen for the current presentation.

As shown in Fig. 1, two high-symmetry cut planes perpendicular to the surface containing the adsorbate allow an almost complete description of the local adsorption geometry of O/Ni(001). Due to the pronounced forward scattering at the adsorbate, only the second layer Ni atom directly below the O will be visible in the obtained images, when normal incidence of the primary beam is used, and the anisotropy of the reference wave remains uncorrected (the so-called searchlight effect[10]). Fortunately, already a rough compensation via the integral kernel K in Eq. (1) makes all additional near-neighbor atoms of the adsorbate show up in the images.[6,12,13] Since the data base parameters concern the algorithm *per se* and not the additional approximate correction for the reference wave anisotropy, we split our investigations into two parts: whereas Sec. IV will concentrate on the influence of data base parameters not yet using the compensating kernel, the effects related to this complementary parameter will be investigated separately in the subsequent section.

When not using a reference wave compensation, no principal difference exists between both cut planes presented in Fig. 1: due to the above-mentioned searchlight effect, only the second layer Ni atom will be accessible for reconstruction in either of them. In the next section the results will hence be demonstrated on the 45° plane only, while it is implicitly understood that all calculations have been performed on the complete 3D volume around the adsorbate.

IV. INFLUENCE OF THE DATA BASE PARAMETERS ON THE ATOMIC IMAGES

The conventional electron detectors in DLEED experiments are able to measure the intensity distribution for polar opening angles up to 50° (full opening up to 100°),[21] whereas simulated patterns are usually calculated over the complete hemisphere. When reducing the angular range of the data input, Fourier transform reasoning would predict a worsening of the lateral resolution of the images and an eventual collapse of the algorithm, if the amount of $\mathbf{k}_\parallel$ information falls below a certain minimum. As illustrated in Fig. 2, the effect of a more and more restricted angular range on the reconstructed cut planes can essentially be understood in this analogous scheme: a 30° opening angle obviously indicates too little data supply, since heavy artifacts are visible apart from the real Ni atom at 2.60 Å below the adsorbate. With increased angular information provided, the images clearly gain in lateral resolution as expected and the disappearance of the artifacts marks the validity of the reconstruction process. However, in the pictures obtained for the two larger angles, the Ni atom exhibits a strong vertical elongation, i.e., a degraded image quality. This phenomenon, which is not expected from Fourier transform theory, is due to the Ni scattering factor: most of the electrons that are detected under large polar angles have undergone fairly large-angle scattering. Since the scattering characteristics of Ni, and of atoms in general, at low energies show a rather complex behavior for such scattering angles (e.g., cusps), these variations disturb the reconstruction algorithm more than the simultaneous benefit of having a larger $\mathbf{k}_\parallel$ range available for the integral. Similar results have been obtained for the related case of photoelectron holography,[22] where the use of a restricted angular range for the SWEEP algorithm had been suggested.[23] Given the above findings, a 50° opening angle seems to be an appropriate compromise between data from a maximized range of $\mathbf{k}_\parallel$ data, without scattering-factor-induced disturbances, and is in any case, the limit of a typical experimental apparatus.[15]

The extension of the energy range up to 435 eV in the simulated data set is of some algorithmic advantage because the energy dependence of the atomic scattering factors becomes weaker with increasing energy. Yet, this advantage is offset by experimental difficulties: at higher energies the data

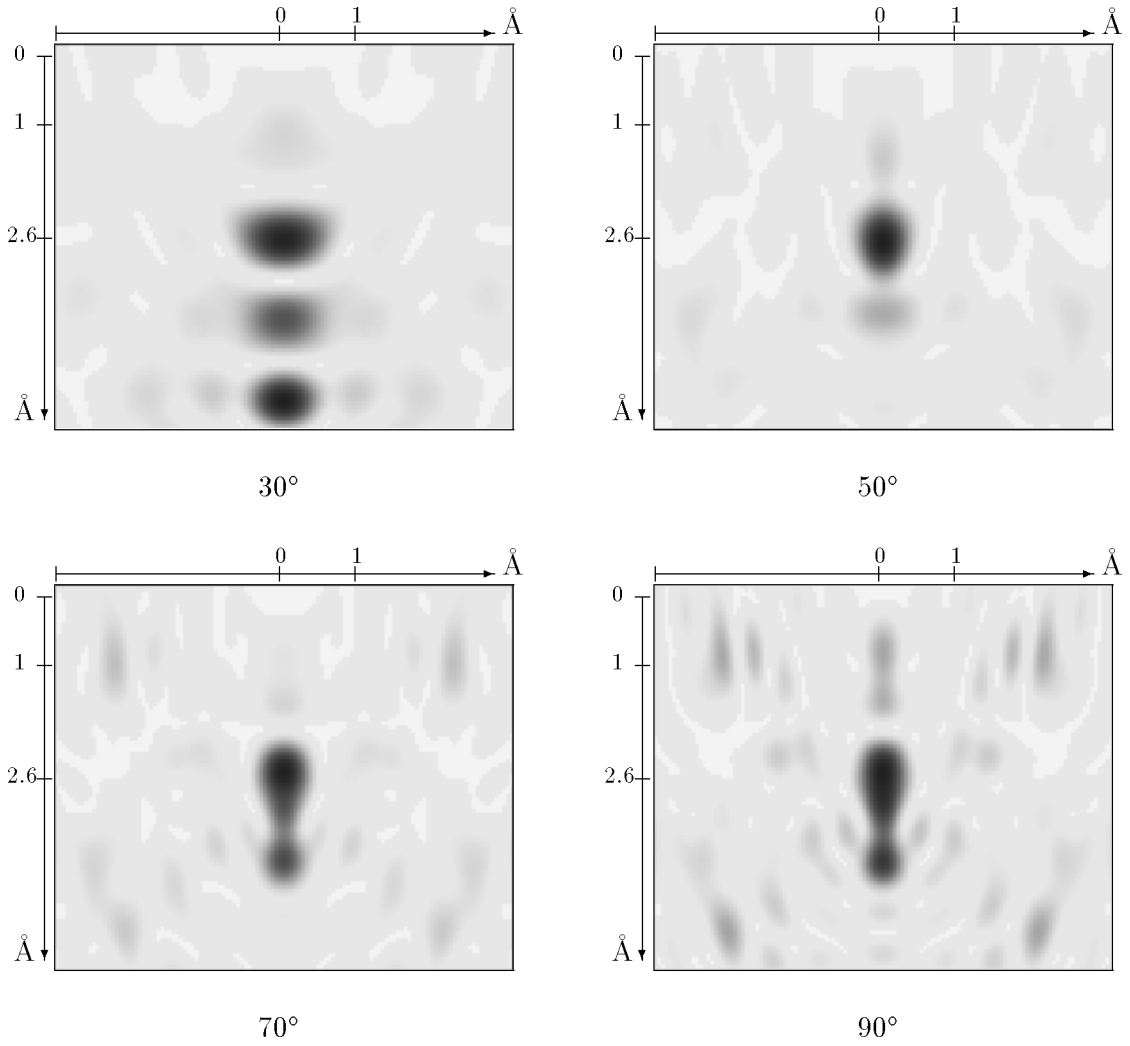

FIG. 2. Reconstructed 45° cut plane for various maximum opening angles using the complete data set between 135 and 435 eV. As also in all following figures, the gray shading corresponds on a linear scale to the calculated intensities, with darker shading corresponding to higher intensities. No threshold for smaller intensities has been used in displaying these images.

acquisition suffers from more closely spaced Bragg spots and eventually from Kikuchi signals,[24] which superimpose the diffuse signal sought. Therefore, an energy range significantly reduced with respect to the above data set has to be selected. In order to check for the proper working of the algorithm on the basis of correspondingly reduced data sets, reconstructions were performed using decreasing sizes of data subsets. Figure 3 shows the results obtained for three different energy ranges using the optimal 50° opening angle. There is a clear influence of the energy width on the image quality, again understandable in terms of the Fourier transform analogue: the smaller the energy range, the worse the achievable vertical image resolution. Equivalent results are found when the lower boundary of the energies used is varied; hence the image resolution appears to depend more on the interval length than on its absolute values. The smallest energy range presented in Fig. 3 additionally indicates an approximate minimum interval for reliable reconstructions, since a further reduction of the data set results in strongly artefficted images. Its order of magnitude ($\simeq$150 eV) fits with the energy range used for the reconstructions performed to date from experimental data,[6,12] thus confirming the general validity.

The influence of data resolution on the reconstructed images appears to be of less importance than the width of the data base: the resolution of the simulated data, i.e., 8×8 points per surface Brillouin zone of the substrate and 13.6 eV energy step width, lies well within the experimental capabilities and is obviously sufficient to produce reliable images of the complete local adsorption geometry. However, even if there is no stringent need to cut down on the resolution, smaller data requirements correspond to fewer experimental measurements and less computing time, and so the corresponding limits are worth investigating. Therefore, calculations were performed using an energy spacing of only 27.2 eV leading to images of just little less quality than before. Only when cutting down to a 40.8 eV grid were severe image distortions found. Thus, the original 13.6 eV steps provide a more than sufficient resolution for the reconstruction algorithm, and hence can be safely used for future data acquisitions. Concerning the angular resolution of the data, no major image degradation was detectable using a 4×4 grid, whereas the 2×2 patterns led to wrong results. However, with parallel detection by video cameras or channel plates at hand the requisite angular resolution is no constraint on the measurement. By application of, e.g., the video technique, a

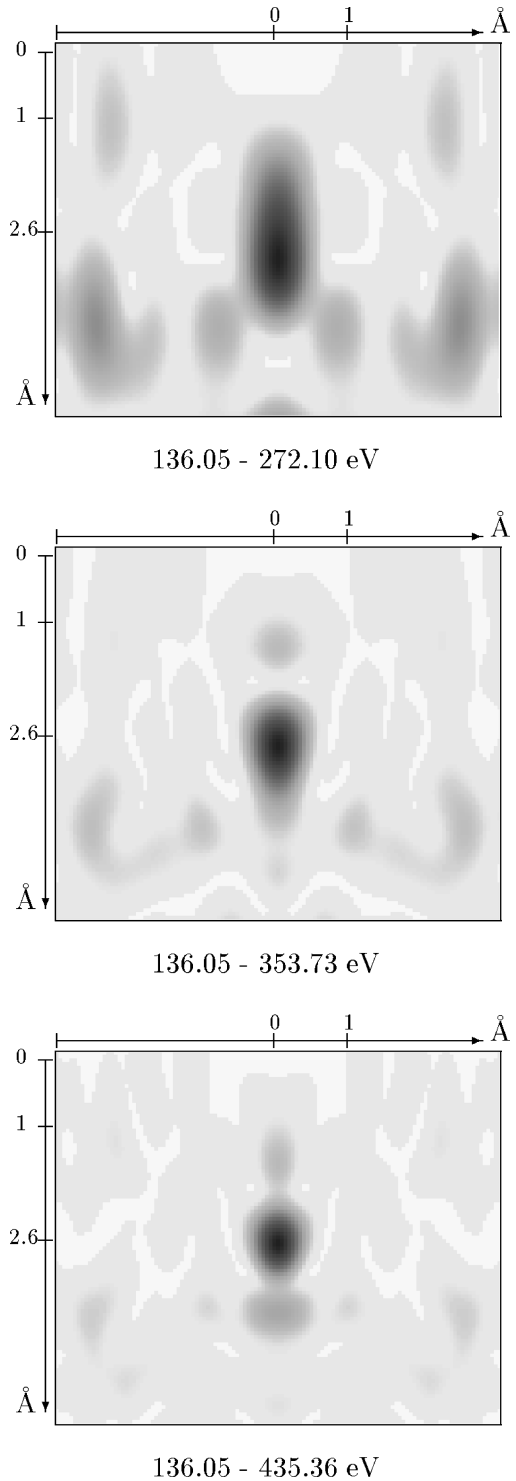

FIG. 3. Reconstructed 45° cut plane for various energy intervals, using a detector opening angle of 50°.

24×24 resolution is routine and was in fact input to recent successful reconstruction procedures from experimental data.[6,12]

V. KERNEL CONSTANT AND CORRECTION FOR REFERENCE WAVE ANISOTROPY

After the above examination of the influence of the data base parameters, we now focus on the reference wave correction. As pointed out above, the searchlight effect caused by the anisotropic atomic scattering factor limits the information obtainable from a data set of one single incidence direction: only atoms lying in the strong forward scattering lobe of the adsorbate are illuminated, and can thus be imaged correctly, while those in other regions around the adsorbate are not accessible by the reconstruction.[10,11] In order to overcome this restriction, Saldin and Chen proposed to correct for the disadvantageous anisotropy of the reference wave by identifying the proper object illumination.[13] For this, two different types of propagation paths from the electron gun towards the adsorbate should be distinguished: in addition to the direct encounter there is the indirect route *via* prior reflection at the substrate. The electrons impinging on the adsorbate in both ways give rise to a scattered joint wave, which travels towards the substrate, thus forming the object illumination. The direct contribution is easily described through the adsorbate's scattering factor, since the incoming field is a simple plane wave. The indirect path, however, is more difficult to grasp as the corresponding wave front on the adsorbate results from the superposition of many different parts arising from reflection at the numerous substrate atoms. As a first approximation, it was argued[13] that it is especially this sum over many contributions that leads to some sort of smearing out and hence justifies the assumption of just an isotropic background due to the indirect illumination. The proposed integral kernel to compensate for the searchlight effect in Eq. (1) thus has the form[13]

$$K(\mathbf{r})=\left[\frac{|f_a(\mathbf{k}_i\cdot\hat{\mathbf{r}})|+C}{r}\right]^{-1}, \tag{4}$$

where $f_a(\mathbf{k}_i\cdot\hat{\mathbf{r}})$ is the atomic scattering factor of the adsorbate, and C is a real constant used to cover the whole indirect part of the illumination. The denominator describes the usual inverse square decay of radiation, which has also been included in all reconstructions presented above without explicit mention.

Despite the remarkably simple approximation of the reference wave, the use of this integral kernel enables reconstructions of high-quality three-dimensional images of the complete adsorption geometry as has already been demonstrated for two different systems using simulated, as well as experimental data.[6,12,13] Nevertheless, the use of a single real constant to represent the whole indirect part of the illumination can only be seen as a first attempt to correct for the reference wave anisotropy and would be expected to be refined in future investigations.

At first glance, the proposed kernel constant C could be seen as a further free parameter in the reconstruction process, due to the difficulty of estimating its value. On the contrary, we will explain in the following that the effect of the constant on the images is clearly defined and, quite importantly, how its optimum value can be derived for a given system. Choosing a very large C for the reconstruction is equivalent to not correcting for the anisotropic reference wave. The corresponding images will consequently contain only the atoms in the searchlight effect restricted area. When reducing the absolute value of C, the images exhibit also atoms in other regions of the local geometry. This is because a smaller C gives more weight to the anisotropic direct illumination and

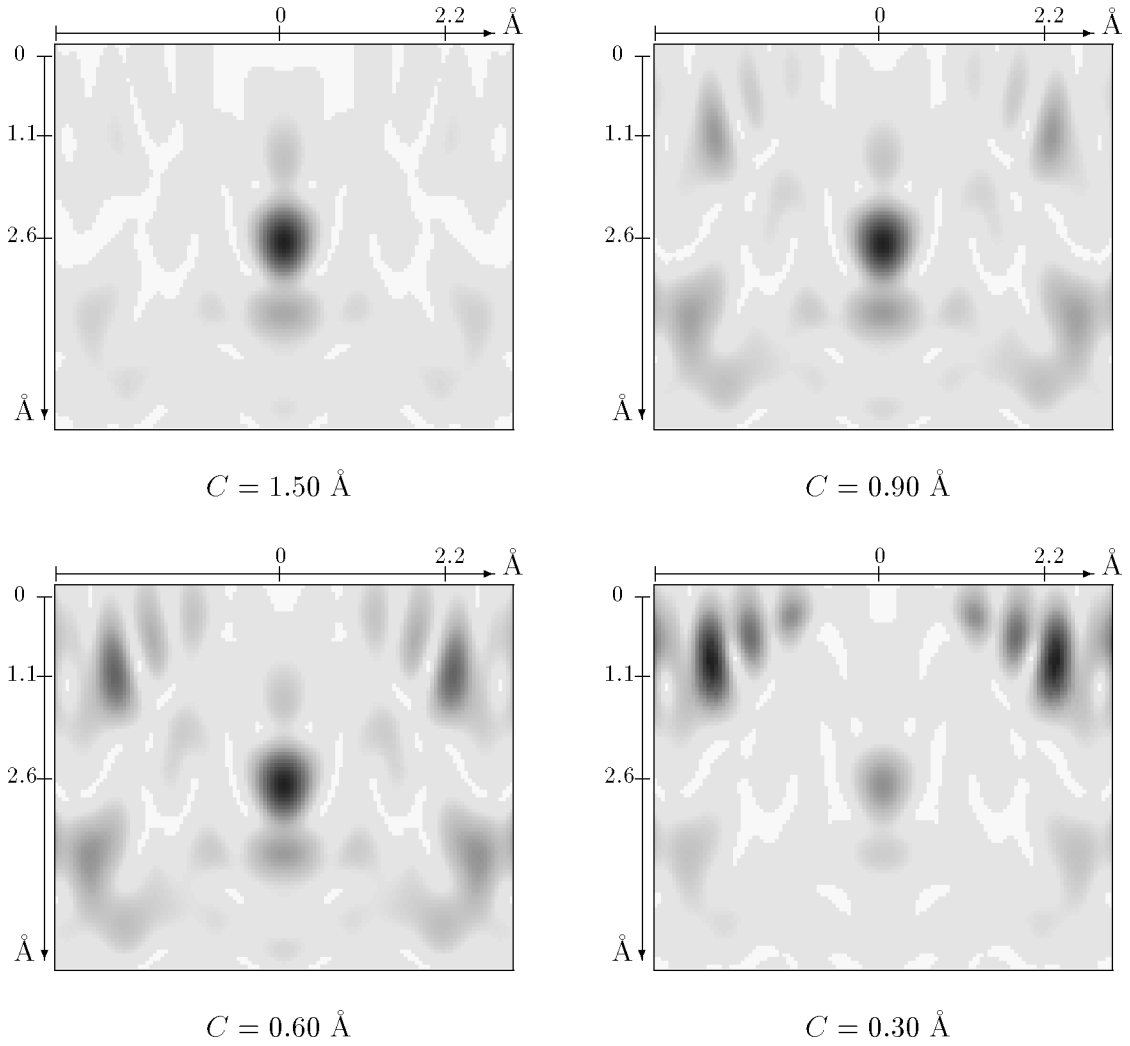

FIG. 4. Reconstructed 45° cut plane for different kernel constants. The complete energy range 135–435 eV was used with a detector opening angle of 50°.

hence corrects more strongly for the reference wave. Finally, for too low a value of C, only atoms outside the forward-lobe directions will be visible, for now the reference wave anisotropy is overcompensated.

This understanding of the effects of the magnitude of C naturally leads to a strategy to determine its optimum value: first, we start with a very large C in order to reconstruct possible atoms in the forward scattering lobe. Subsequently, we reduce the constant to reconstruct further substrate atoms. This strategy applied to reconstruction from the simulated O/Ni(001) data is documented in Fig. 4, where a series of 45° cut planes for varying constants is depicted. For the largest C no differences due to the use of the kernel are apparent in the image in comparison to those obtained without the use of a kernel. By slowly reducing the value of C, the effects outlined above show up: the previously invisible first layer Ni atoms appear slowly, just to be the only bright points left when C becomes too small. As is apparent, the price of the approximation of the indirect illumination by a simple constant can be seen as additional artifacts in the image for the smallest kernel constant. The use of the CORRECT kernel necessitates hence a certain level of caution: due to its current simplicity, it can provide only somewhat approximate information. This is also evident from the fact that the first layer Ni atoms are found at positions 0.5 Å too far out, whereas the second layer atom visible without kernel is shifted by only 0.1 Å from its correct position.

Nevertheless, when optimizing all data base and additional parameters in the manner described, the CORRECT algorithm is able to produce an impressive view of the complete local geometry from the simulated data. This is illustrated in Fig. 5, where a value of C has been chosen, which produces the different atoms with approximately equal intensity (indicating the optimum compensation of the reference wave anisotropy). Also included is the 3D visualization of the results to demonstrate how easily understandable and clear is the reconstructed information from DLEED holography.

VI. THE BRAGG-SPOT PROBLEM

As a last untreated discrepancy between simulated and experimental data we need to examine the influence of the Bragg spots on the reconstruction process. Since the DLEED

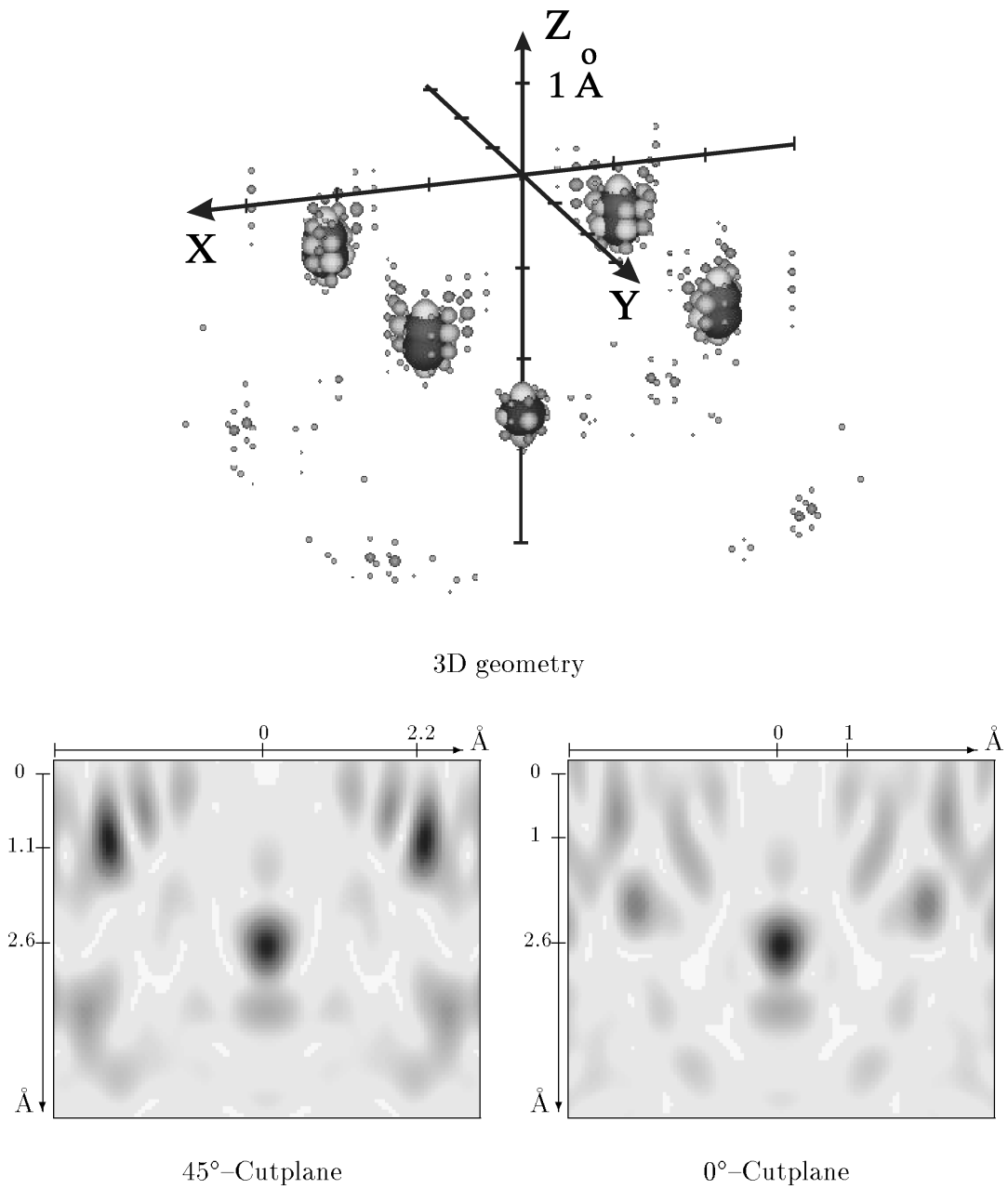

FIG. 5. Reconstructions for optimized data input: complete energy range, 50° opening angle, and kernel constant of $C=0.45$ Å. Upper part: 3D view of the complete adsorption geometry. The adsorbate is at the origin of the 3D Cartesian coordinate system. The intensity at each voxel is represented by a sphere whose radius is proportional to the intensity, and whose gray shading varies from white for the lower values to black for the higher ones. Lower part: 45° and 0° cut planes—to be compared with the schematic view in Fig. 1.

program[20] used for the simulated patterns calculates only propagation paths involving at least one scattering at the adsorbate, even the intensities with $\mathbf{k}_{\parallel}$ values corresponding to integer-order substrate spots contain exclusively DLEED intensities. In contrast, the experimental diffraction intensities at such values of $\mathbf{k}_{\parallel}$ are dominated by the intensities from purely substrate scattering processes, leading to the high-intensity substrate Bragg spots. The usual procedure for dealing with this problem has been simply to cut out a certain area around the spots.[6,11,12] However, with the Fourier transform analogue so far being surprisingly predictive, one might become wary of cutting out areas in a pattern producing residual sharp edges, which are additionally located at periodic positions. Also, if the area cutout becomes too large, the image reconstruction procedure must break down due to insufficient data input.

To check the quantitative influence on the images, circular areas of different sizes around Bragg-spot positions were removed from the simulated data. The corresponding cut planes, reconstructed under otherwise optimized parameters, are shown in Fig. 6 together with sample diffraction patterns to visualize the cutting procedure. As suspected, a clear degradation of the image quality develops with the appearance of strong artifacts. Fortunately, these artifacts only become dominant and so prevent a clear identification of the adsorption geometry, when the cutout radius is much larger than

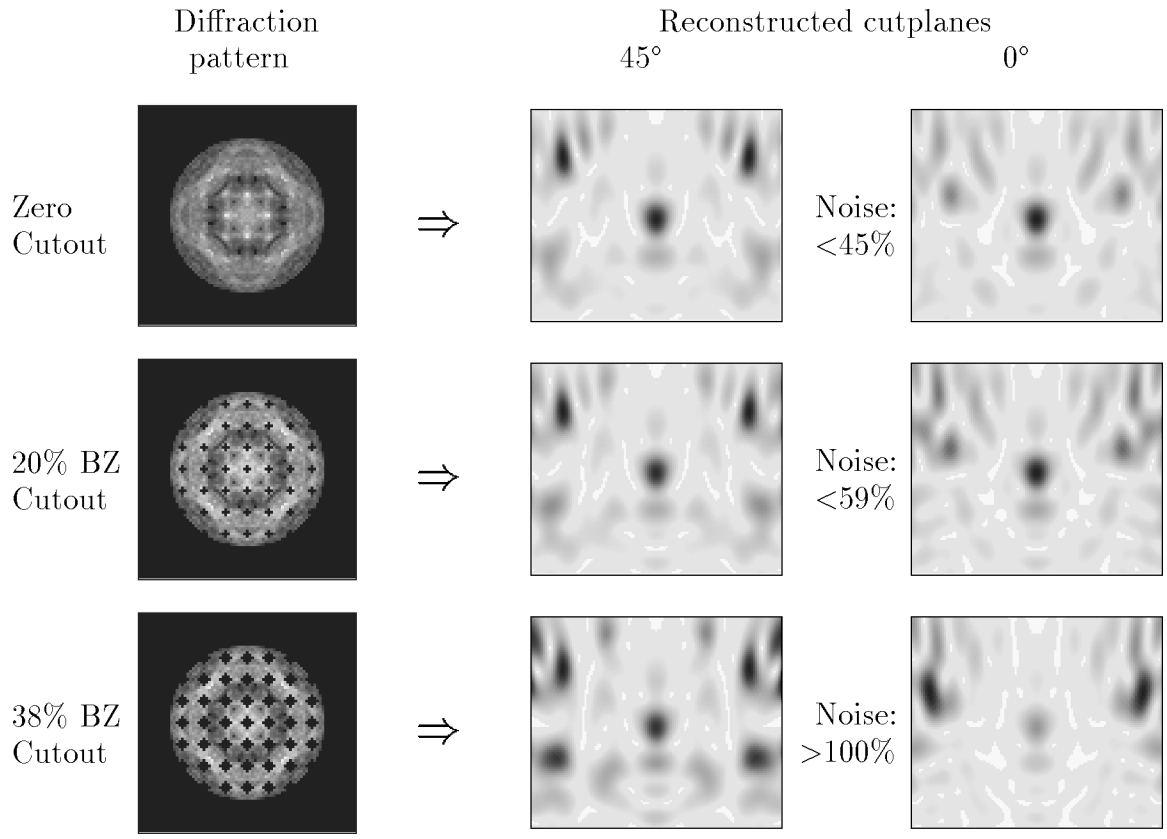

FIG. 6. Reconstructions for different Bragg-spot cutouts using the otherwise optimized parameter constellation of Fig. 5. Left panels: example diffraction pattern showing the varying circular cuts. Middle and right panels: corresponding 45° and 0° cut planes. The noise indicates the highest intensities not associated with atom positions.

that normally necessary for experimental data. For previous reconstructions,[12,6] this Bragg-spot radius was usually found to be of the order of 20% of the Brillouin-zone width, and hence is comparable to the middle scenario in Fig. 6, where reliable images are still possible. Nevertheless, our results stress that the Bragg spots pose a problem, which has to be treated with much care. Future investigations should therefore be made on how to improve the simple removal to a procedure more compatible with a Fourier-transform-like algorithm.

VII. CONCLUSIONS

In the present paper, the influence of various parameters on the reconstruction process in holographic diffuse LEED was investigated. In order to circumvent experimental uncertainties, simulated diffuse intensities were used, as calculated for the adsorption system O/Ni(100). As this system exhibits no special structural features, the results obtained should hold also for other atomic adsorption phases.

We first concentrated on the four data base parameters (energy and angular range, and energy and angular resolution) describing the discrete and finite data base used as input to the holographic integral transform. It was found that a 50° polar collecting angle as provided by most display-type LEED optics yields the best images, while an approximate energy width of 150 eV marks a minimum for reliable reconstructions. Concerning the resolution of the data, a sampling grid of 8×8 points per Brillouin zone is sufficient and might even be reduced to 4×4. Also the energy step width may be as large as 27.2 eV (1 hartree), though we recommend working with a value of about 10 eV ($\approx$0.5 hartree) to be on the safe side.

With the additional reference wave correction included in the CORRECT algorithm the kernel constant C is introduced as another variable. By examination of its influence on the image quality, a way to determine its best value is proposed. It represents a compromise that avoids the appearance of the searchlight effect (values too large) and of substantial image artifacts, plus disappearing atoms due to an overcompensation of the adatom's scattering anisotropy (values too small). In particular, the best C in the case of the simulated O/Ni(001) data was found to be 0.45 Å.

As a last step, the removal of experimental Bragg-spots intensities, which carry no holographic information, was discussed. Though the simple cutting out of these signals is dangerous from the Fourier point of view, because sharp edges appear on a regular grid, nevertheless this is the routine procedure at the moment. In the present investigation, no major disturbances in the images appeared, when the Bragg-spot cutout was limited to 20% of the Brillouin zone at maximum, which is compatible with common experimental data.

Using a parameter constellation according to the above guidelines, a clear and impressive image of the complete 3D adsorption geometry could be reconstructed from simu-

lated data for a single direction of incidence. The results retrieved are thought to offer suitable guidelines for the data collection, data processing, and the performance of the reconstruction algorithm. This should be of help for the reliable image reconstruction from diffuse intensity distributions also for unknown systems of atomic adsorbates supplying a first and direct visualization of the adsorption geometry.

ACKNOWLEDGMENTS

The Erlangen group acknowledges support through the Deutsche Forschungsgemeinschaft (DFG). D.K.S. is likewise grateful to the National Science Foundation (Grant No. DMR-9320275) and to the Donors of the Petroleum Research Fund, administered by the American Chemical Society.

[1] J. B. Pendry, *Low Energy Electron Diffraction* (Academic, London, 1974).
[2] M. A. Van Hove, W. H. Weinberg, and C.-M. Chan, *Low Energy Electron Diffraction* (Springer-Verlag, Berlin, 1986).
[3] K. Heinz, Rep. Prog. Phys. **58**, 637 (1995).
[4] J. B. Pendry and K. Heinz, Surf. Sci. **230**, 137 (1990).
[5] D. K. Saldin and P. L. De Andres, Phys. Rev. Lett. **64**, 1270 (1990).
[6] D. K. Saldin, X. Chen, J. Vamvakas, M. Ott, H. Wedler, K. Reuter, K. Heinz, and P. L. De Andres, in Proceedings of the 5th International Conference on the Structure of Surfaces (ICSOS-5), [Surf. Rev. Lett. (to be published)].
[7] (a) L. J. Terminello, J. J. Barton, and D. A. Lapiano-Smith, Phys. Rev. Lett. **70**, 599 (1993); (b) J. G. Tobin, G. D. Waddill, H. Li, and S. Y. Tong, *ibid.* **70**, 4150 (1993).
[8] (a) H. Li, S. Y. Tong, D. Naumovic, A. Stuck, and J. Osterwalder, Phys. Rev. B **47**, 10 036 (1993); (b) D. K. Saldin, G. R. Harp, and X. Chen, *ibid.* **48**, 8234 (1993).
[9] (a) Z.-L. Han, S. Hardcastle, G. R. Harp, H. Li, X.-D. Wang, J. Zhang, and B. P. Tonner, Surf. Sci. **258**, 313 (1991); (b) I. H. Hong, P. R. Jeng, S. C. Shyu, Y. C. Chou, and C. M. Wei, Surf. Sci. Lett. **312**, 743 (1994).
[10] C.-M. Wei and S. Y. Tong, Surf. Sci. **274**, L577 (1992).
[11] C.-M. Wei, S. Y. Tong, H. Wedler, M. A. Mendez, and K. Heinz, Phys. Rev. Lett. **72**, 2434 (1994).
[12] D. K. Saldin, K. Reuter, P. L. De Andres, H. Wedler, X. Chen, J. B. Pendry, and K. Heinz, Phys. Rev. B **54**, 8172 (1996).
[13] D. K. Saldin and X. Chen, Phys. Rev. B **52**, 2941 (1995).
[14] J. B. Pendry and D. K. Saldin, Surf. Sci. **145**, 33 (1984).
[15] U. Starke, J. B. Pendry, and K. Heinz, Prog. Surf. Sci. **52**, 53 (1996).
[16] K. Heinz, R. Döll, M. Wagner, U. Löffler, and M. A. Mendez, in Proceedings IVC-12/ISS-8, The Hague 12 [Appl. Surf. Sci. **70/71**, 367 (1993)].
[17] J. J. Barton, Phys. Rev. Lett. **61**, 1356 (1988).
[18] (a) J. J. Barton and L. J. Terminello, *The Structure of Surfaces III*, edited by S. Y. Tong *et al.* (Springer, Berlin, 1991); (b) J. J. Barton, Phys. Rev. Lett. **67**, 3106 (1991).
[19] E. O. Brigham, *The Fast Fourier Transform and its Applications* (Prentice-Hall, Englewood Cliffs, NJ, 1988).
[20] D. K. Saldin and J. B. Pendry, Comput. Phys. Commun. **42**, 399 (1986).
[21] (a) K. Heinz, Rep. Prog. Phys. **58**, 637 (1995); (b) K. Müller and K. Heinz, Springer Ser. Surf. Sci. **2**, 105 (1985).
[22] (a) S. Y. Tong, C. M. Wei, T. C. Zhao, H. Huang, and H. Li, Phys. Rev. Lett. **66**, 60 (1991); (b) H. Huang, H. Li, and S. Y. Tong, Phys. Rev. B **44**, 3240 (1991).
[23] S. Y. Tong, H. Li, and H. Huang, Phys. Rev. B **46**, 4155 (1992).
[24] M. A. Mendez, C. Glück, M. Wagner, U. Löffler, R. Döll, and K. Heinz, Surf. Sci. **290**, 45 (1993).